Hindawi Publishing Corporation
Journal of Polymers
Volume 2013, Article ID 183463, 17 pages
http://dx.doi.org/10.1155/2013/183463

Research Article

Investigation of Cure Reaction, Rheology, Volume Shrinkage and Thermomechanical Properties of Nano-TiO_2 Filled Epoxy/DDS Composites

Jyotishkumar Parameswaranpillai,[1] Abhilash George,[1] Jürgen Pionteck,[2] and Sabu Thomas[3,4]

[1] *Department of Polymer Science and Rubber Technology, Cochin University of Science and Technology, Cochin, Kerala 682022, India*
[2] *Leibniz-Institute for Polymer Research Dresden, Hohe Strare 6, 01069 Dresden, Germany*
[3] *School of Chemical Sciences, Mahatma Gandhi University, Priyadarshini Hills, Kottayam, Kerala 686560, India*
[4] *Centre for Nanoscience & Nanotechnology, Mahatma Gandhi University, Priyadarshini Hills, Kottayam, Kerala 686560, India*

Correspondence should be addressed to Jyotishkumar Parameswaranpillai; jyotishkumarp@gmail.com

Received 26 March 2013; Accepted 2 July 2013

Academic Editor: Jae-Woon Nah

The cure reaction, rheology, volume shrinkage, and thermomechanical behavior of epoxy-TiO_2 nanocomposites based on diglycidyl ether of bisphenol A cured with 4,4′-diaminodiphenylsulfone have been investigated. The FTIR results show that, at the initial curing stage, TiO_2 acts as a catalyst and facilitates the curing. The catalytic effect of TiO_2 was further confirmed by the decrease in maximum exothermal peak temperature (DSC results); however, it was also found that the addition of TiO_2 decreases the overall degree of cure, as evidenced by lower total heat of reaction of the cured composites compared to neat epoxy. The importance of cure rheology in the microstructure formation during curing was explored by using rheometry. From the PVT studies, it was found that TiO_2 decreases the volume shrinkage behavior of the epoxy matrix. The mechanical properties of the cured epoxy composites, such as tensile strength, tensile modulus, flexural strength, flexural modulus, impact strength, and fracture toughness of the polymer composites, were examined. The nanocomposites exhibited good improvement in dimensional, thermal, and mechanical properties with respect to neat cross-linked epoxy system. FESEM micrographs of fractured surfaces were examined to understand the toughening mechanism.

1. Introduction

Epoxy resins are widely used in industrial applications, such as matrices in composite materials, and for aerospace applications, adhesives, coating, electronic circuit board-laminates, and so forth due to their excellent mechanical and thermal properties, low cost, ease of processing, fine adhesion to many substrates, good chemical resistance, good weathering resistance, low specific weight, and long pot life period [1]. The major problems with epoxy are low stiffness and low strength compared to metals and also cured epoxy resins are highly brittle, which greatly limits their application in some areas [2]. Toughness reinforcement of epoxy resins has attracted considerable attention for over the last 30 years. A new approach aiming to overcome this basic problem is related to nanotechnology and uses fillers in the nanometer scale. Nanoparticles embedded in polymer matrix have attracted increasing interest because of the unique mechanical, optical, electrical, and magnetic properties displayed by the nanocomposites [3]. Nanoparticles can significantly alter the mechanical properties of the polymer close to a particle surface due to the changes in polymer chain mobility. The enhancement in toughness is attributed to the size of the nanoparticles, since they can provide high specific surface area which helps to develop new material behaviour and is determined by interfacial interactions, resulting in unique properties and completely new classes of materials [4, 5]. Recently many researchers have shown that the addition of nanofillers not only increases the toughness but also strengthens the obtained composites [6–8].

The cure kinetics and reaction mechanisms of various epoxy monomer and its nanocomposites with nanofillers have been studied using different methods including FTIR spectroscopy [9, 10], and DSC [11, 12]. FTIR and DSC have been a useful technique for studying cure kinetics of crosslinking reactions in thermosetting epoxy. FTIR spectral analysis is based on the band intensity change of the functional group during the reaction time at a given temperature. In DSC analysis, both the isothermal and the dynamic heating experimental modes have been used extensively to determine the cure kinetic models and their parameters for the neat epoxy and epoxy/nanocomposites, which are mostly cured with amine curing agent. The basic assumption is that the heat evolution monitored and recorded by DSC is proportional to the extent of consumption of the functional groups, such as the epoxide groups in the epoxy resin or amine groups in the curing agent [13].

The processing of the thermoset matrix composites is more complicated and less controlled because of their reactivity. In this processes, polymer synthesis and shaping take place in a single operation; this involves the conversion of liquid monomers or polymers into solid crosslinked polymers [14, 15]. In addition, tendency of polymers to expand or contract during processing is a problem that has been widely recognized, especially for epoxy systems [16, 17]. Thus, the knowledge of rheology and volume shrinkage behavior of the epoxy resin system is particularly necessary to have a correct control of the processing mechanism and the subsequent engineering design.

The very high specific surface area of nanoparticles, however, causes the nanoparticles to attract each other due to van der Waals forces and to form agglomerates with dimensions of several micrometers [6]. It is reported that a considerable amount of improvement in mechanical properties can be achieved using very low amounts of nanofiller loadings [7, 8]. To extract maximum benefit from their high specific surface, nanoparticles have to be homogenously dispersed in the polymer matrix to increase the effective interfacial surface between the fillers and the matrix. The mechanical properties significantly depend on the dispersion of the particles in the matrix. This interfacial surface allows a good transfer of the applied load from the matrix to the nanoparticles. Good dispersion also results in a more uniform stress distribution and minimizes stress concentration which should increase the general strength and modulus of the composites [18, 19]. Nanoparticles are generally introduced into the polymer matrix by various techniques which include application of high shear forces during mechanical stirring [7, 20–22], pulsed ultrasound vibrations [23], and direct incorporation with chemical methods [24, 25]. This avoids the agglomerated state.

Nanoscaled TiO_2 has gained great interests in the last decades because of its unique properties and good performance. The TiO_2 is extensively used in industry, such as additives for epoxies, plastics, and rubbers [6, 26–30]. Moreover, TiO_2 filled polymers are well-known antimicrobial materials [31–35]. Since epoxy is a very common material for aerospace and automotive industry, addition of TiO_2 may act as substitute for pollution treatment (in presence of UV light, TiO_2 generates hydroxyl radicals, which can degrade or oxidize the pollutants into more environmentally friendly products) and disinfectant (photo catalytic degradation of bacteria and grime) [35] which is a major industrial issue. TiO_2 is well known for photo chemical degradation of toxic chemicals, UV shielding, waste water purification, and so forth. Apart from that, it is widely used in piezoelectric capacitors, solid oxide fuel cells, electrode materials in lithium batteries, energy converter in solar cells, and so forth [36].

Very few studies have been reported on the epoxy/TiO_2 nanocomposites, most of them are focused on the final mechanical properties [37, 38]. However, the effect of TiO_2 on cure, rheology, and volume shrinkage of epoxy systems has never been investigated. In this context, a detailed study in this topic is very important. In this paper, we present an experimental investigation on the effect of mechanically dispersed TiO_2 on the network formation of an epoxy/amine system. The effect of TiO_2 on the volume shrinkage was also examined. Finally, we have investigated the thermomechanical properties of the cured epoxy/TiO_2 nanocomposites.

2. Experimental Part

2.1. Materials Used. The epoxy resin, diglycidyl ether of bisphenol-A (DGEBA) (Lapox L-12, Atul Ltd, India.) was used as the matrix material. The amine hardener, diamino diphenyl sulfone (DDS) (Lapox K-10, Atul Ltd., India.), was used as a cross-linker for the epoxy. Nano-TiO_2, with size around 100 nm, was obtained from Riedel-de Haen (product code: 14027), Germany.

2.2. Preparation of Epoxy/TiO_2 Nanocomposites. TiO_2 nanoparticles were dispersed in DGEBA (epoxy) and mixed at 180°C using a high speed magnetic stirrer for two hours; then a stoichiometric amount of DDS with an epoxy: amine ratio of 2 : 1 was added as the curing agent and mixed well. The solution was transferred to an open mold. The composites were cured in the open mold at 180°C for three hours and then postcured at 200°C for 2 hours. Composites with TiO_2 contents of 0, 1, 5, and 10 g in epoxy-hardener mixture (100 g DGEBA + 35 g DDS) were prepared, and the samples were named as neat epoxy, 0.7 wt% TiO_2, 3.6 wt% TiO_2, and 6.9 wt% TiO_2, respectively.

For fourier transform infrared spectrometer (FTIR), differential scanning calorimetry (DSC), rheology and pressure-volume-temperature (PVT) observations, the freshly prepared mixtures were immediately used or stored before use in a freezer at −20°C. For other experiments, the freshly prepared mixtures were cured in the air oven at 180°C for 3 h and then postcured at 200°C for further 2 h. The resultant composites were then allowed to cool slowly to room temperature.

3. Characterization

3.1. Fourier Transform Infrared Spectroscopy. In situ curing studies were carried out using a fourier transform infrared-spectrometer EQUINOX 55 (Bruker Optik GmbH). A few

milligrams of sample were placed in a sample holder and *in-situ* FTIR measurements were performed at 150°C for three hours. Please note that at 180°C the reaction between epoxy and amine is too fast to be followed by *in-situ* FTIR analysis.

3.2. Differential Scanning Calorimetry . The noncured samples were analyzed using a DSC Q1000 of TA-Instruments. Samples of about 6 mg were encapsulated in aluminum pans. Modulated DSC measurements were carried out in the temperature range from −60°C (5 min.) to 300°C (0.5 min.) at a heating rate of 2 K/min. in N_2 atmosphere with an amplitude of ±0.31 K and a period of 40 s. Please note that at higher heating rates the curing reaction was not complete up to 300°C. Above this temperature beginning degradation (proven by TGA investigations, which are not shown here) overlaps the curing reaction. Thus, to ensure complete curing below 300°C the low heating rate had to be used in this work. The heat of the reaction (ΔH) was determined from the total heat flow of the 1st heating scan. The curing enthalpy is proportional to the extent of the reaction. In the composites, the measured curing enthalpy ΔH is normalized to the epoxy content ($\Delta H_{(\mathrm{corr})}$).

3.3. Oscillatory Shear Rheology. Rheological properties of the TiO_2/epoxy/amine mixtures during isothermal curing were studied by the oscillatory shear measurements using a stress-controlled ARG2 rheometer (TA Instruments). Due to the complete vitrification of the samples, a disposable parallel plate system was utilized. The system consisted of two aluminium plates of 25 mm, one standard upper plate and one lower plate with drip channel, which were replaced at the end of each measurement. Temperature control was achieved by a sealed environmental testing chamber (ETC system, TA Instruments). All experiments were carried out with 5% strain and an angular frequency of 1 Hz and were used to determine the storage modulus (G', Pa), loss modulus (G'', Pa), tan δ, and complex viscosity (η^*).

3.4. Pressure-Volume-Temperature Analysis. The PVT measurements were done using a fully automated GNOMIX high pressure mercury dilatometer. Below 200°C the absolute accuracy of the instrument is of 0.002 cm^3/g. In practice, the change in specific volume as small as 0.0002 cm^3/g can be resolved reliably. The cross-linking reaction was characterized in the so-called data acquisition mode (DAQ) at 10 MPa and 180°C by following the volume shrinkage of the samples as a function of time. In order to check whether any cross-linking has taken place during the sample preparation stages, the experimental initial specific volumes were compared with those calculated initial specific volumes from the densities of the individual components by assuming an additive behavior (Table 1). The experimental specific volumes and calculated specific volumes are comparable, or in other words, the deviation was within an acceptable range (1%), this means that no curing or little curing takes place during sampling.

3.5. Scanning Electron Microscopy. Each sample was cooled and fractured in liquid nitrogen so that the morphology of the composites will not be effected. After that the samples were sputtered with gold in the Leica EM SCD050 sputter coater (Germany) to avoid the charging effect. Finally the sputtered samples were analyzed by using a Hitachi S-4800 high-resolution scanning electron microscope (Japan) with an accelerating voltage of 1 kV.

Table 1: Experimental and calculated initial specific volume epoxy/TiO_2 composites at 180°C.

Samples	Specific volume (experimental) cm^3/g V_{E0}	Specific volume (calculated) cm^3/g V_{T0}
Neat epoxy	0.893	0.900
3.6 wt% TiO_2 nanocomposite	0.827	0.827

3.6. Transmission Electron Microscopy. Due to the low penetration power of electrons, in order to be able to see the nanoparticle filler distribution under the sample surface, it is necessary to mount objects for examination in the electron microscope as very thin films. Therefore, samples were cut by using an ultramicrotome (ULTRACUT E. from Reichert-Jung (Germany)) into 50 to 80 nm thick ultra thin films. The prepared samples were examined in an EM 902 transmission electron microscope (Zeiss, Germany) with an accelerating voltage of 80 kV.

3.7. Thermogravimetric Analysis. Thermal stability of the blends was analyzed by thermogravimetric analyser (TGA). TA Instrument Mettler Toledo TGA/SDTA/851 (USA) was used to monitor the samples. The measurements were performed on 3–5 mg of the samples from room temperature to 700°C at a heating rate of 20°C/min and under nitrogen atmosphere.

3.8. Thermomechanical Analysis. The thermomechanical properties of neat epoxy and epoxy/TiO_2 composites were measured using a TA Instruments, Co., Q 400 thermomechanical analyser (USA). The samples were scanned from 50 to 250°C at a heating rate of 1°C/min. Rectangular specimens of 20 × 10 × 3 mm^3 were used for the analysis.

3.9. Dynamic Mechanical Analysis. The investigation of the viscoelastic properties was performed using dynamic mechanical analyzer (DMA 2980, TA Instruments, Co.), USA. Rectangular specimens of 40 × 10 × 3 mm^3 were used. The analysis was done in single cantilever mode at a frequency of 1 Hz, from –100 to 300°C and at a heating rate of 1°C/min.

3.10. Tensile Properties. Specimens for mechanical testing were machined to the required dimensions from the cast panels with a cutting machine. Tensile measurements were performed according to ASTM D 638. The measurements were taken with a universal testing machine (Tinius Olsen, Co.) Model H 50 KT (UK) at a cross-head speed of 10 mm/min. Rectangular specimens of 100 × 10 × 3 mm^3

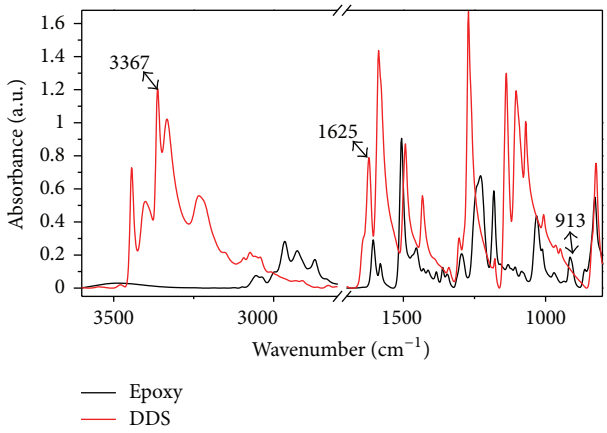

Figure 1: FTIR spectra of epoxy monomer and DDS.

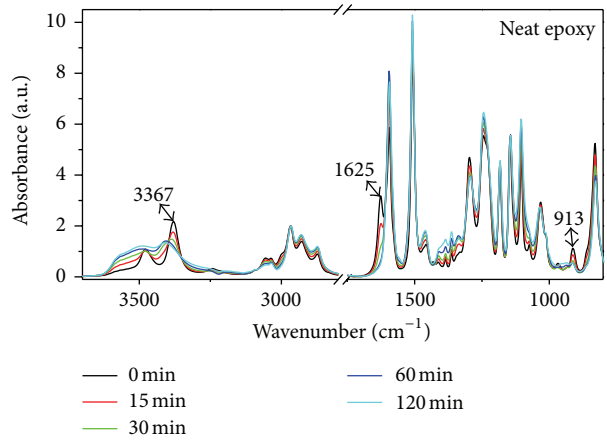

Figure 2: FTIR spectra of neat epoxy/DDS system us a function of reaction time ($T = 150^{\circ}$C).

were used for determining the tensile strength. The tests were performed on 6 different specimens of the same sample and the mean values were calculated.

3.11. Flexural Properties. The flexural measurements were performed according to ASTM D 790. The cross-head speed was 10 mm/minute. The measurements were taken with a universal testing machine (Tinius Olsen Co) Model H 50 KT (UK) at a cross-head speed of 10 mm/min. Rectangular specimens of $100 \times 10 \times 3\,\text{mm}^3$ were used. The flexural modulus was calculated from the slope of the initial portion of the flexural stress-strain curve. The tests were performed on 6 different specimens of the same sample and the mean values were calculated.

3.12. Impact Strength. Charpy impact strength of the unmodified and modified epoxy resin was measured by means of a Charpy impact test following the specifications ISO 179/1eA. Impact tests were performed on a Zorn Stendal impact testing machine (Germany). The dimensions of the specimens were approximately $40 \times 8 \times 4\,\text{mm}^3$. At least 10 successful measurements were used to obtain the mean values.

3.13. Fracture Toughness. Fracture toughness of the specimens was determined according to ASTM D 5045-99. The measurements were taken with a universal testing machine Zwick (UPM—Z010) (Germany). Rectangular specimens of 60 mm length, 10 mm width, and 4 mm thickness were used for fracture toughness measurements. A notch of 5 mm was made at one edge of the specimen. A natural crack was made by a fresh razor blade at the base of the notch. The analysis was done in bending mode at room temperature. At least six successful measurements were used to obtain the mean values.

3.14. Field Emission Scanning Electron Microscopy. The morphology of the fractured surface of crosslinked epoxy as well as epoxy nanocomposites, after the K_{Ic} test, was examined using a ULTRA FESEM, (model-ultra plus) Nano Technology Systems Division Carl Zeiss SMT AG, Germany. The samples were coated with platinum by vapor deposition using a SCD 500 Sputter Coater (BAL-TEC AG, Liechtenstein).

4. Results and Discussion

4.1. Spectroscopic Analysis. Figure 1 shows the FTIR spectra of epoxy monomer and DDS. From the FTIR spectra, the most remarkable peaks are those of the amine region of DDS. We have strong peaks for the NH_2 groups from the DDS at 1625 and 3367 cm^{-1} [39]. The intense signal of the epoxy ring is centered at 913 cm^{-1} due to the asymmetrical ring stretching, in which the C–C bond stretches during the contraction of the C–O bond [39].

Figure 2 reveals the FTIR spectra of pure epoxy/DDS mixture at different stages of cure. The epoxide band at 913 cm^{-1} is very evident at the beginning of the experiment ($t = 0$). The intensity of epoxide band reduces with curing time and is almost not detectable after 90 minutes, indicating the time for the consumption of epoxy groups. On the other hand, the strong absorbances at 1625 and 3367 cm^{-1} of the NH_2 groups from the DDS also reduce with curing time and almost disappear after 90 minutes, again indicating the time for complete epoxy/amine conversion. However, an evaluation of the curing kinetics is difficult since during polymerization the spectrum between 3100 and 3600 becomes complex; the unreacted amines and hydroxyl groups overlap to a broad band and the absorbance at 1625 cm^{-1} forms after short curing time a shoulder to the strong absorption at 1594 cm^{-1} caused by phenyl ring [40]. Therefore, the rate of epoxy/amine polymerization was estimated only by following the loss of epoxide band intensity with respect to cure time.

Figure 3 shows the FTIR spectra of the 3.6 wt% TiO_2 containing epoxy nanocomposite. As in the pure epoxy/DDS system the band at 913 cm^{-1} is very evident at the beginning of the experiment ($t = 0$) and reduces with curing time. Again, after 90 min. it almost disappears. The rate of epoxy/amine polymerization can be estimated by following the loss of epoxide band intensity with respect to cure time. In Figure 4,

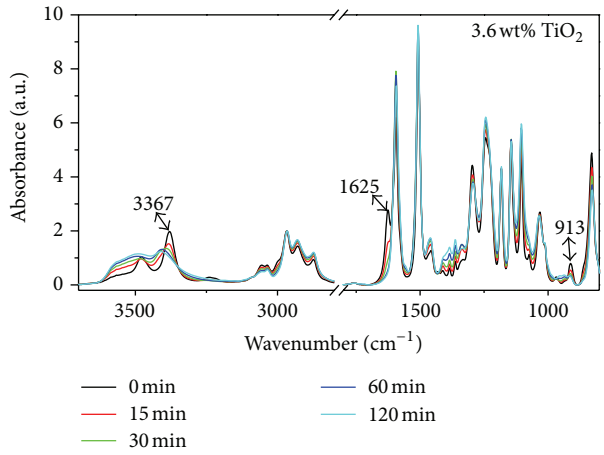

Figure 3: FTIR spectra of 3.6 wt% TiO_2 modified epoxy/DDS system using a function of reaction time ($T = 150^{\circ}C$).

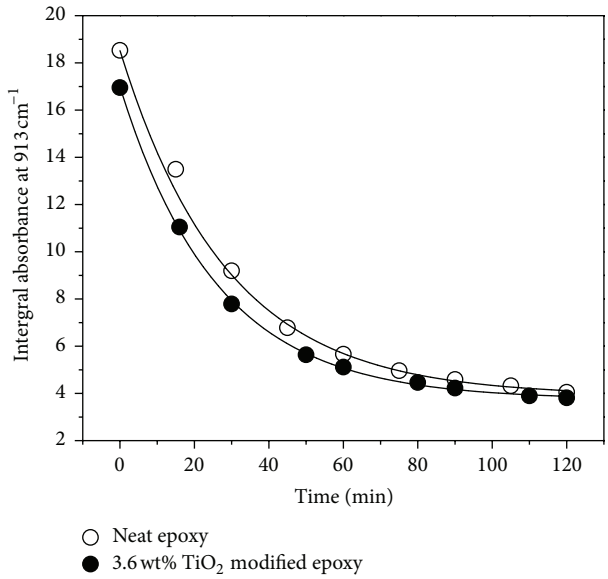

Figure 4: Exponential decay behavior of epoxy resin in epoxy/amine mixture during curing (dot is corresponding to the experiment data, and line corresponding to the result simulated by $y = y_0 + A_1 \exp(-x/t_1)$) ($T = 150^{\circ}C$).

we compare the loss of epoxy band with respect to cure time for the pure epoxy/DDS system and 3.6 wt% TiO_2 containing epoxy nanocomposite studied. We observe similar behavior for both systems that is a rapid decrease of epoxide band intensity within the first 45 min, followed by a slower decrease in the next hour. However, the band does not completely disappear and the intensity levels off.

To evaluate the cure reaction in more detail, the loss of epoxide band with respect to cure time was simulated with Maxwell's decay equation [41] (Figure 4):

$$y = y_0 + A_1 \exp\left(-\frac{x}{t_1}\right). \quad (1)$$

Table 2: First-order decay constants for nanocomposites.

Specimen	t_1 (min)	y_0	A_1	R^2
Neat epoxy	30.42 ± 1.81	3.71 ± 0.24	15.04 ± 0.34	0.997
3.6 wt% TiO_2 nanocomposite	26.08 ± 0.55	3.75 ± 0.06	13.26 ± 0.11	0.999

Table 3: $\Delta H_{t\,(\mathrm{Corr})}$ and T_p for the TiO_2/epoxy composites.

Samples	ΔH_t (J/g)	$\Delta H_{t\,(\mathrm{Corr})}$ (J/g)	T_p (°C)
Neat epoxy	−394	−394	179
0.7 wt%	−353	−355	176
3.6 wt%	−354	−367	176
6.9 wt%	−328	−352	177

As $t \to \infty$, $y \to y_0$. Here A_1 is a constant and t_1 is the relaxation time of the cure reaction and indicates the rate of the epoxy/amine reaction. As shown in Figure 4, the simulation results gave a good fit to the experimental data. The fit parameters t_1, A_1, y_0, and R^2, to assess the quality of fit, are given in Table 2. The relaxation time t_1 decreases with filler addition due to the acceleration of the epoxy/amine reaction by the presence of TiO_2 particles. The increase in reaction rate was supposed to be from the high thermal conductivity and high specific surface area of the TiO_2 particles.

4.2. Nonisothermal Cure Behavior. Figure 5 shows differential scanning calorimetry thermograms during the curing of composites as obtained during first heating in modulated DSC scan. For any given specimen, only one (exothermic) DSC peak was observed due to the polymerization of DGEBA/amine, owing to the heat evolved when epoxy rings are opened during their reaction with amine functionalities. The peak area under the baseline extrapolated at the end of the reaction was used to calculate the total heat of reaction (ΔH). The maximum exothermal peak temperature (T_p) and the ΔH_{corr} values, normalized to the epoxy weight content, as a function of TiO_2 concentration, are reported in Table 3. From the Table it is clear that TiO_2 act as catalyst and facilitate curing at the initial stage by lowering T_p; on the other hand, ΔH_{corr} tends to be smaller as higher the TiO_2 content. This is because the addition of TiO_2 dilutes the epoxy-DDS reaction volume and also the presence of TiO_2-epoxy interactions reduces the crosslinking degree attained by the polymer matrix.

4.3. Rheological Analysis. For the in-depth understanding of cure process, oscillatory shear flow measurements were performed under isothermal condition at three different temperatures (150, 165, and 180°C) to investigate the rheological parameters of epoxy nanocomposites. The rheological profile remains the same irrespective of the temperature. For avoiding overlapping of the results, we are giving only the representative rheological profile obtained at 180°C. In the rheological characterization of thermosets, the oscillatory shear flow measurements are preferred to those of the steady

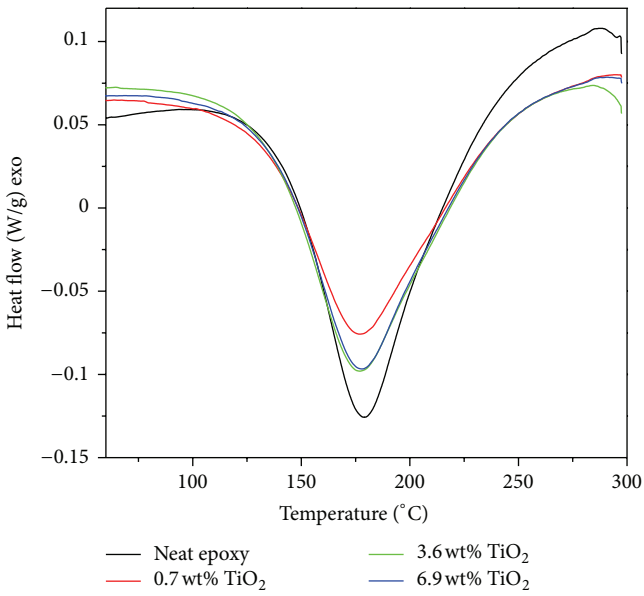

FIGURE 5: Variation of heat flow with respect to temperature.

shear because they can be applied to a material not only in the liquid state but also in rubbery and glassy.

The profile of change in complex viscosity as a function of cure time at 180°C is shown in Figure 6(a). At the beginning of the curing, the viscosity slowly increases with time, and then, at a certain point a rapid increase in viscosity is observed. The reaction between epoxy and amine induces various chemical and physical phenomena; the cross-densification advances and hence resin viscosity increases. Moreover, this increase in complex viscosity curves shifted to shorter times with TiO_2 addition due to better epoxy/amine reaction by the acceleration effect caused by TiO_2 particles. The growth of the complex viscosity follows first-order exponential equation:

$$y = y_0 + A_1 \exp\left(\frac{x}{t_1}\right). \tag{2}$$

Figure 6(b) reveals the variation of rheological parameters ($\tan\delta$, G', and G'') as a function of real time/conversion scale in case of neat epoxy system at 180°C. The $\tan\delta$ value during the initial stages of cure is around 90, indicating the liquid nature of the material [42]. As the curing progresses, a rapid drop in the $\tan\delta$ is observed corresponding to the chemical gelation of the material. This behavior is typical for epoxy systems [43].

From Figure 6(b), during the early stages of the reaction, G' is below G'' indicating the liquid nature of the material, after some time both G' and G'' increase with the linear growth of the epoxy chains. This is followed by a crossover point (gelation point) where G' equals G'' that means the system acts as both elastic and viscous, storing and dissipating an identical amount of energy at this point [14, 42]. Epoxy composites with, 0.7, 3.6, and 6.9 wt% TiO_2 follow a similar trend. Figure 6(c) shows the rheological profile of the 3.6 wt% TiO_2 containing epoxy composites, which is representative for all other nanocomposites studied.

In the present study, three criteria for gelation time where applied to the dynamic mechanical data. First criterion is time at $G' = G''$, second criterion is the time at the decrease in $\tan\delta$ [44, 45]. A third criterion for gel point is to locate the time at which the viscosity reaches a value of 10^3 Pa·s [46]. For accuracy, we make use of all the criteria to evaluate the gel point and taken the average of all to determine the precise gelation point to calculate the activation energy. On the other hand, two criteria for vitrification time where applied, for accuracy. First criteria is time at minimum $\tan\delta$ and the second criteria is time at maximum G''. The gelation and vitrification times calculated from the rheological profiles at different isothermal temperatures are listed in Table 4. The gelation and vitrification time of the epoxy/amine system decreases with the addition of TiO_2 particles. The cure acceleration effect caused by TiO_2 could bring positive effect on the processing of composite since it needs shorter pre-cure time and postcure time.

In order to characterize gelation and vitrification as a function of temperature and time, a TTT diagram is proposed. The concept of a time-temperature-transformation (TTT) cure diagram has been developed by Gillham and Babayevsky [47] for polymer systems and represents the time required to reach gelation and vitrification during an isothermal cure. The TTT diagram for the 0.7 wt% TiO_2 is proposed in Figure 6(d). The transition from viscous to elastic gel is produced by the gelation transition. On the other hand, transition from elastic gel to completely crosslinked glass produced by the vitrification transition. From the TTT diagram, it is clear that the behavior of the epoxy monomer depends on the cure temperature.

For better evaluation of the effect of TiO_2 content on rheology, activation energies for polymerization were obtained from gelation times, by using the following differential equation [48, 49]:

$$\frac{dx}{dt} = A \exp\left(-\frac{E_a}{RT}\right) f(x), \tag{3}$$

where A is the preexponential constant, E_a is the activation energy, R is the gas constant, and T is the absolute temperature. The extent of the reaction is independent of the cure temperature.

Integration of this equation from $x = 0$ to $x = x_{gel}$ by using natural logarithm leads to

$$\ln \int_0^{x_{gel}} \frac{dx}{f(x)} = \ln A + \ln\left(t_{gel}\right) - \left(\frac{E_a}{RT}\right). \tag{4}$$

Based on Flory theory [50] the extent of reaction at gel point is constant, so the previous equation can be expressed as

$$\ln\left(t_{gel}\right) = \text{constant} + \frac{E_a}{RT}. \tag{5}$$

Thus, from the slope of the plot regarding the linear relationship between $\ln(t_{gel})$ and the inverse of temperature the apparent activation energy can be calculated.

The values of $\ln(t_{gel})$ obtained by the rheological tests are plotted against $1/T$ in Figure 6(e). The activation energies

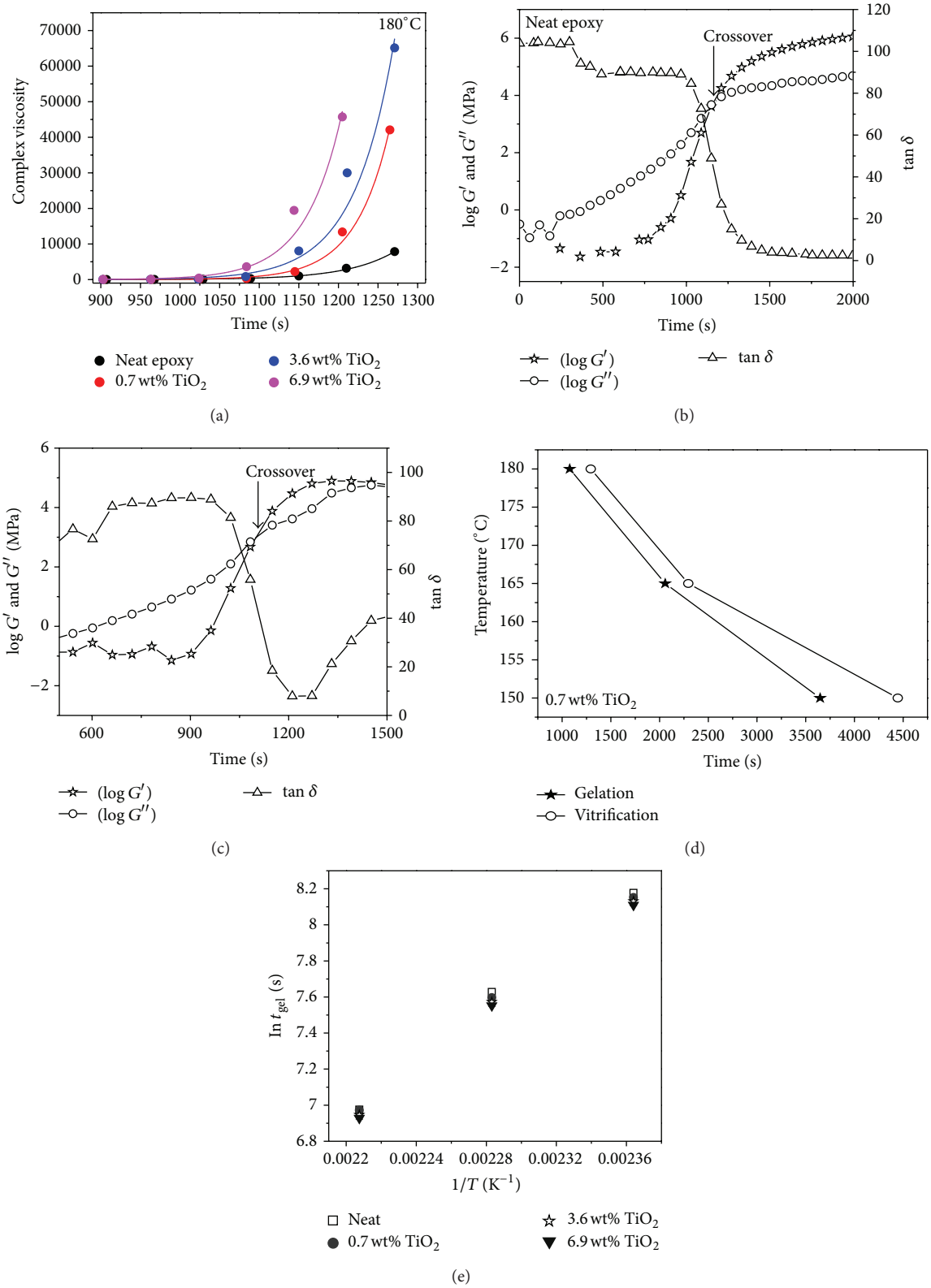

FIGURE 6: (a) Exponential growth behaviors of complex viscosity during curing of epoxy/TiO_2 nanocomposites at 180°C (dot is corresponding to the experiment data and line is corresponding to the result simulated by $y = y_0 + A_1 \exp(x/t_1)$). (b) Rheological profile of neat epoxy at 180°C. (c) Rheological profile of 3.6 wt% TiO_2/epoxy nanocomposites at 180°C. (d)Times to gelation and vitrification for 0.7 wt% TiO_2 modified epoxy system. (e) Variation of ln (t_{gel}) from complex viscosity with cure temperature for the neat matrix and epoxy nanocomposites.

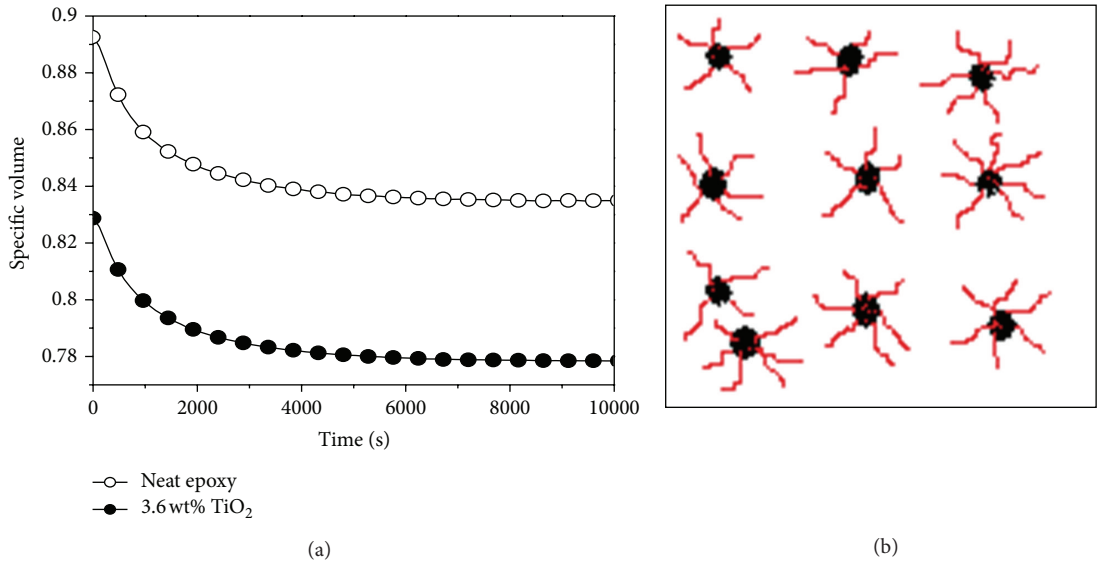

FIGURE 7: (a) Specific volume versus curing time from PVT test (epoxy/TiO_2 composites) at 180°C, 10 MPa. (b) A schematic representation of constrained layer of polymer chains around the TiO_2 nanoparticles dispersed in the epoxy matrix (white-epoxy matrix, black-TiO_2. particles, red-constrained polymer chains).

have been established from the plot. The activation energy values are 65 ± 5, 63 ± 3, 63 ± 2, and 63 ± 2 for neat epoxy, 0.7 wt% TiO_2/epoxy, 3.6 wt% TiO_2/epoxy, and 6.9 wt% TiO_2/epoxy composite, respectively. In comparison to amine cured DGEBA epoxy, the amine cured DGEBA/TiO_2 composites exhibit lower activation energies. These results validate our FTIR and DSC studies.

4.4. Pressure Volume Temperature Studies. The typical isothermal curing of thermoset/TiO_2 based composites is accompanied by the polymerization shrinkage and vitrification of the thermoset-rich phase. The material shrinkage that occurs during curing can adversely affect the desired tolerance of the final product and hence a PVT study is necessary for thermosetting composites. Pressure-volume-temperature characterization is a well-known tool for the investigation of change in specific volume with respect to cure time for epoxy systems. Figure 7(a) gives the change in specific volume data obtained for neat epoxy/DDS and 3.6 wt% TiO_2/epoxy/DDS mixtures with respect to cure time. The absolute specific volume decreases with TiO_2 content due to the higher dense TiO_2 nano filler in the epoxy matrix. A temperature of 180°C and a pressure of 10 MPa were applied for 13 hours, during which a sharp decrease in the specific volume was observed for both neat epoxy and composite due to the *in-situ* epoxy-amine reaction (volume shrinkage) [51–53]. After heating for three hours, the specific volume reached a constant value for composites. The beginning of the final plateau region corresponds to the vitrification process, although at this stage the curing reaction could continue slowly.

The change in specific volume is 0.05847 cm^3/g and 0.05061 cm^3/g for pure epoxy and epoxy composites, respectively, and is a indirect measure of volume shrinkage. Decrease in volume shrinkage for epoxy/TiO_2 composites can be explained as follows. The addition of TiO_2 dilutes the epoxy-DDS reaction volume. Moreover, presence of dense TiO_2 nano filler may increase the viscosity of the system and hence progressively decrease the relative volume shrinkage. Moreover, due to the high surface to volume ratio of nano TiO_2, epoxy polymer/oligomer get attached to the filler surface, which generates a constrained polymer around the filler surface as depicted in Figure 7(b). These constrained layer of polymer chains does not or only slightly undergo shrinkage due the presence of rigid TiO_2 particles.

4.5. Micro- and Nanostructure of the Nanocomposites

4.5.1. Scanning Electron Microscopy (SEM). The surface morphology of the cured nanocomposites was investigated by SEM. SEM micrographs were taken for all the composites. Figure 8(a) shows the SEM micrograph of the neat epoxy system which reveals a single phase. Even though, we broke the sample in liquid nitrogen, the surface morphology of neat epoxy look fractured because of the brittle nature of the control epoxy. On the other hand SEM micrograph with 0.7 wt% TiO_2 filler content (Figure 8(b)) is flat and smooth and quiet nicely form line boundaries at the interface between the pure epoxy matrix. The filler catalyses the epoxy polymerization and crosslinking and the interfaces are the contact areas of the approaching polymerization front. The apparent roughness of the surface increases with TiO_2 content. Figure 8(c) shows a SEM micrograph of the 3.6 wt% TiO_2 modified epoxy which reveals a similar morphology as observed for 0.7 wt% TiO_2 filler content. When the concentration was increased to 6.9 wt% TiO_2, particles are more agglomerated, (Figure 8(d)), [24]. As mentioned before even though the neat epoxy was fractured in liquid nitrogen there was observed fracture step

edges due to the highly brittle nature of the material. On the other hand, fracture step edges are absent in the case of composites with 0.7 wt% TiO_2 and 3.6 wt% TiO_2 due to increased ductility of the epoxy matrix.

4.5.2. Transmission Electron Microscopy. For better understanding of the dispersion of the TiO_2 in the epoxy matrix, TEM micrographs were taken. TEM is a straightforward technique to visualize quality of the dispersion of nanoparticles within epoxy matrix. The micrographs obtained from the sections of the nanocomposites reveal the presence of individual TiO_2 particles embedded in the epoxy matrix. Figure 9(a) shows a TEM image of the neat epoxy; it is homogeneous with a single phase; Figure 9(b) shows a TEM image of epoxy modified with 0.7 wt% TiO_2; there were a few agglomerates. The size of the particles varies around 100 nm. A similar morphology was observed for 3.6 wt% TiO_2 and 6.9 wt% TiO_2 modified epoxy system (Figures 9(c) and 9(d)) but agglomerates of particles appear. The particle agglomerates are due to weak van der Waals attraction forces, which are higher for smaller particles leading them to poor dispersion.

4.6. Thermal Stability. Thermal stability of the neat epoxy and TiO_2 nanocomposites was studied by TGA. TGA and DTG (derivative thermogram) curves for all the cross-linked composites are given in Figures 10(a) and 10(b), respectively. From the thermograms (Figure 10(a)) nano TiO_2 filled composites show relatively less thermal decomposition than the neat crosslinked epoxy. In general, the decomposition started at around 350°C and was completed at around 500°C. The average weight loss of around 1-2% up to 300°C is due to the release of moisture if any. On the other hand, the weight loss above 350°C is related to the decomposition of the polymer. The main degradation peak in the composites occurred between 390 and 470°C, where 70%–80% of the degradation occurred. Beyond the main degradation stage, all the volatile materials were driven off from the sample resulting in the residual char. The % residual of the composites was better than the neat epoxy due to the presence of the thermally stable TiO_2 particles. For better understanding the thermal stability of the nanocomposites, their weight percentage at different temperatures were taken and are given in Table 5; it would immediately point out that for temperatures up to 400°C (the first 4 rows) little difference appears for different loaded composites. On the contrary, above 400°C (500 to 700°C) the stabilizing effect of the filler becomes clear, each column value is greater than that of the column on the left. The final (at 700°C) mass percent lefts from Table 5 are 12.5, 17.3, 19.2, and 23.7 for the loadings of 0, 0.7, 3.6 and 6.9 wt%, respectively. It means that, in the first case, still a left mass from neat matrix is 12.5: if we add the mass left to the different loading, in the next values, such as to obtain, roughly, $12.5 + 0.7 = 13.2, 12.5 + 3.6 = 16.1, 12.5 + 6.9 = 19.4$. If we substrate the final (at 700°C) mass percent left with these calculated values, then we have $17.3 - 13.2 = 4.1, 19.2 - 16.1 = 3.1, 23.7 - 19.4 = 4.3\%$; this suggest that % residual of the composites was better that neat epoxy system. The temperature at which decomposition rate has its maximum can be calculated from the DTG curves, shown in Figure 10(b). The thermal stability of composites is more evident from DTG curves where the main degradation for composites is comparatively smaller than that of the neat epoxy, while the main degradation temperature remains unaffected.

4.7. Thermomechanical Analysis. Thermal expansion behaviour of the nanocomposites was measured using a TMA to investigate the effect of TiO_2 on the dimensional change of the epoxy nanocomposite samples. The TMA thermograms of cured epoxy nanocomposites are shown in Figure 11. From the thermograms, the dimensions increase with increase in temperature is visible. During heating, the nanocomposites expand and then undergo a glassy-to-rubbery transformation (T_g) (at around 200°C); it then continues to expand in the rubbery phase with a greater liner expansion coefficient, showing the normal expansion behaviour of rubber state. In neat epoxy system drop in the dimension change near to T_g was observed. The observed drop in the dimension change near to T_g is due to relaxation of below T_g frozen nonequilibrium states of the cured samples [53]. It is important to mention that the inserted NPs or the associated mixing avoided the freezing of such local sites in the nanocomposites. From the plot, it can be concluded that the dimensional stability of crosslinked epoxy remains unaltered by the addition of nanoparticles.

4.8. Dynamic Mechanical Analysis. The storage modulus demonstrates strength and the stiffness. Figure 12(a) shows the storage modulus curves of the epoxy composites. From the profile, the storage modulus values of the epoxy nanocomposites were higher than the neat crosslinked epoxy for all temperatures. The rigid TiO_2 particles improved the stiffness of the epoxy matrix composites, especially for 6.9 wt% TiO_2 modified epoxy nanocomposites. There is an inflection point at around 200°C which indicates the transition from the solid state to the rubbery state, that is, the glass transition (T_g) of the system. Loss modulus curves (Figure 12(b)) indicate the energy dissipation and can be used to measure the viscous component of the material. The loss modulus is greater for the composites, the dispersed TiO_2 dissipates energy due to resistance against viscoelastic deformation of the surrounding epoxy matrix. Only one peak is observed for the entire system, the peak corresponds to the T_g of the crosslinked epoxy phase. It is important to mention that the peak is observed at lower temperature for the composites, which indicates slightly reduced crosslinking density for the composites.

4.9. Mechanical Tests. Tensile tests were conducted to measure the stress–strain behavior of different wt% nanocomposites under uniaxial tension. The stress-strain behavior from the tensile tests is given in Table 6. It can be seen that addition of filler shows slight improvement in the tensile properties of the epoxy system. The modulus, strength, and ductility were approximately stable, with fluctuations for the ductility

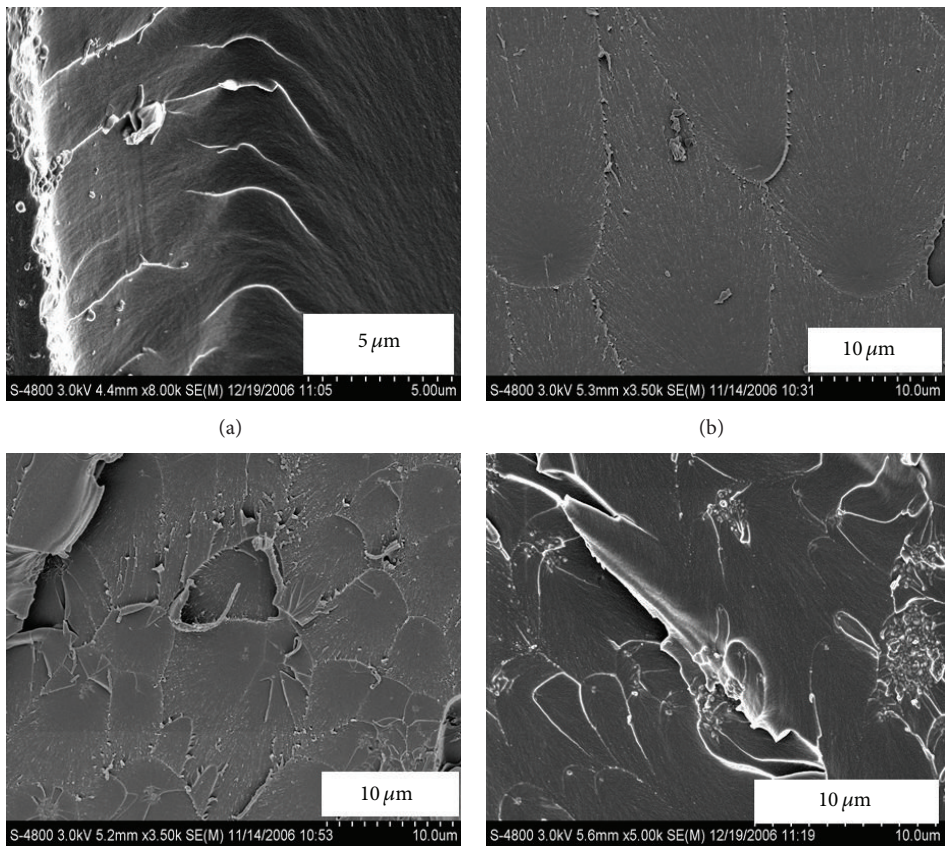

Figure 8: SEM micrographs of epoxy nanocomposites; (a) neat epoxy, (b) 0.7 wt% TiO_2, (c) 3.6 wt% TiO_2, and (d) 6.9 wt% TiO_2.

Table 4: Gelation and vitrification times for the TiO_2/epoxy composites.

T (°C)	Gelation time (sec) of the epoxy phase			Average of all the three parameters (s)	Vitrification time (sec) of the epoxy phase	
	($G' = G''$) (s)	tan δ Max (s)	η^* (s)		tan δ (s)	Max G'' (s)
			Neat epoxy			
150	4015	3580	3568	3721	4653	4853
165	2266	2048	2139	2151	2476	2536
180	1146	1000	1147	1097	1571	1452
			0.7 wt% TiO_2 composites			
150	3939	3534	3470	3648	4415	4475
165	2174	2008	1992	2058	2295	2295
180	1145	1024	1066	1078	1265	1323
			3.6 wt% TiO_2 composites			
150	3906	3587	3397	3630	4235	4186
165	2137	1986	1943	2022	2415	2475
180	1101	1000	1039	1047	1211	1271
			6.9 wt% TiO_2 composites			
150	3954	3558	3328	3613	4355	4417
165	2115	1941	1905	1987	2356	2356
180	1057	952	1021	1010	1144	1205

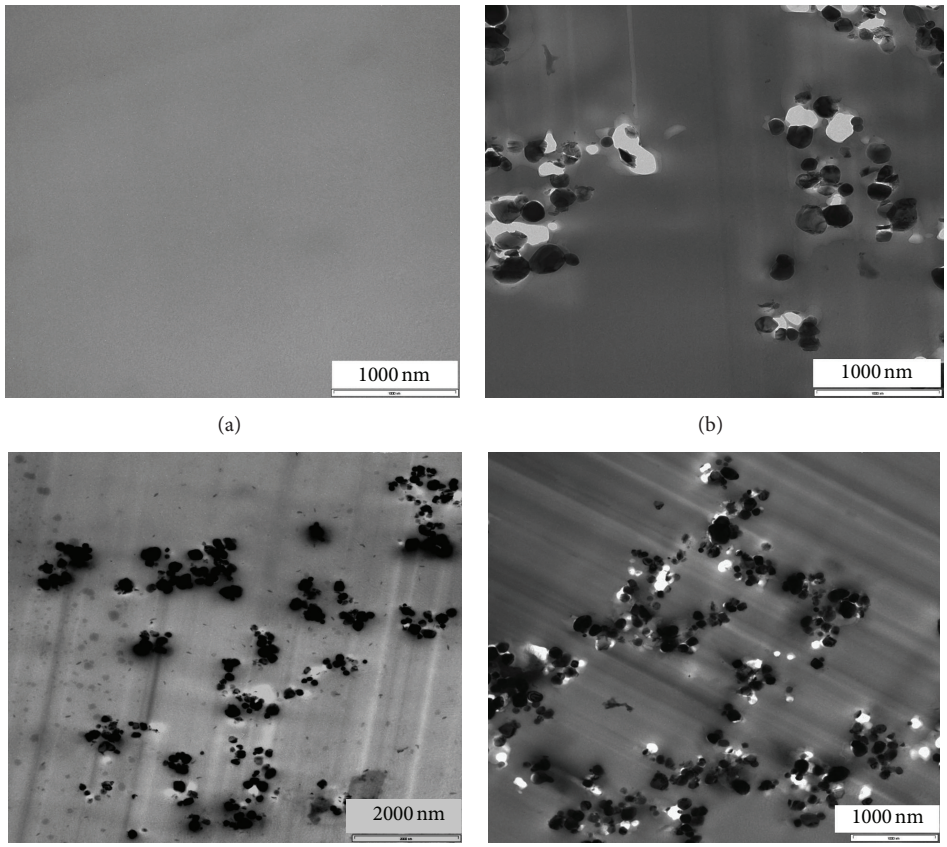

Figure 9: TEM micrographs of epoxy nanocomposites; (a) neat epoxy (b) 0.7 wt% TiO_2, (c) 3.6 wt% TiO_2, and (d) 6.9 wt% TiO_2.

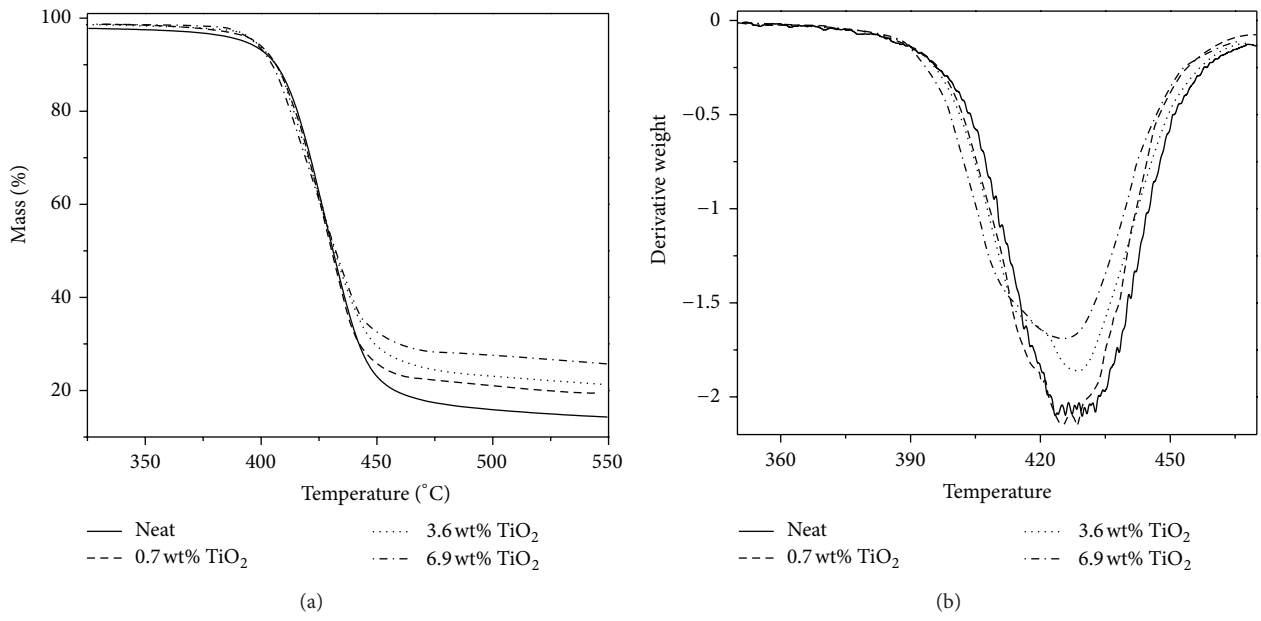

Figure 10: (a) TGA curves for epoxy nanocomposites. (b) DTG curves for epoxy nanocomposites.

Table 5: TGA data of epoxy composites at different temperatures.

Temperature (°C)	% residue			
	Neat	0.7 wt% TiO_2	3.6 wt% TiO_2	6.9 wt% TiO_2
100	99.5	99.7	99.7	99.8
200	98.2	98.9	98.9	99.1
300	98.0	98.7	98.7	98.7
400	93.1	94.2	94.1	93.5
500	15.9	20.8	22.9	27.2
600	13.4	18.3	20.2	24.8
700	12.5	17.3	19.2	23.7

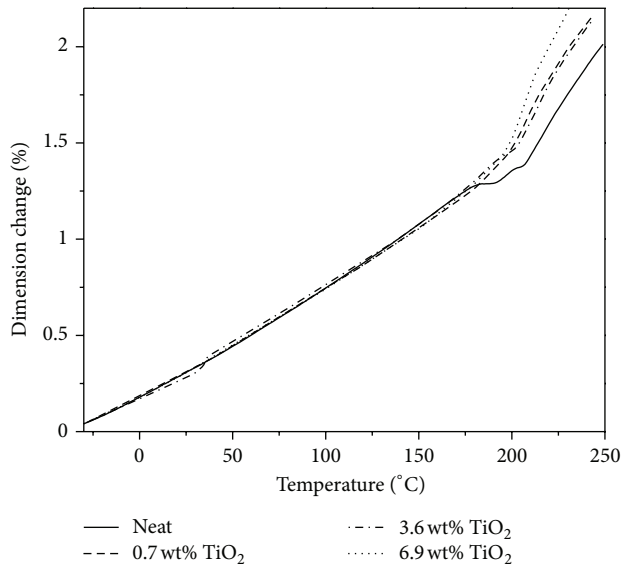

Figure 11: TMA curves for epoxy nanocomposites.

and an apparent moderate increase (10%) for modulus and strength.

The flexural properties of the epoxy composites are given in Table 7. With filler addition, the modulus increased; particularly with 6.9 wt% TiO_2 addition, on the other hand, the % strain and strength decreased. The flexural load is a combination of tensile and compressive load, and therefore compressive modulus should be increased by addition of stiff fillers; one could expect that the flexural modulus would rather increase with TiO_2 addition. When the composites were subjected to flexural bending, the TiO_2 particles are not able to transfer the applied load but hinder the movement of epoxy resins molecular chains. This leads to stress within the materials, so that the bend fracture strength of material decreases [36].

The impact toughness of a material describes the energy required to break the specimen. The magnitude of the impact strength reflects the ability of the material to resist impact. The impact strength of the cross-linked epoxy and epoxy composites is shown in Figure 13. Addition of TiO_2 particles enhanced the impact strength of the neat epoxy slightly, but not for 6.9 wt% TiO_2. The increase in the impact strength can be attributed to the increased toughness of the matrix upon filler addition. The nanometer-sized TiO_2 particles with good dispersion are able to block the propagation of cracks through the polymer. This is assigned to the reinforcing effect of nano-TiO_2. The impact properties of polymers are mainly enhanced by small particles with low aspect ratio, since large particles can act as crack initiation sites. However, large filler content (6.9 wt%) made it more difficult for dispersion and easier for nanosized particle to "agglomerate." Since agglomerated particles make it possible to generate defects, stress concentration will likely occur within the epoxy due to external force, resulting in decreased impact strength.

Nanocomposites simultaneously improve the fracture toughness as well as the stiffness of a neat polymer. The resistance of a material to crack initiation and propagation can be explained in terms of fracture toughness. We express the fracture toughness of the cured epoxy resin and its composites in terms of the stress intensity factor K_{IC}. The value of the stress intensity factor (K_{IC}) was calculated using (1) [41]:

$$\text{Stress intensity factor}, K_{IC} = \frac{QPa^{1/2}}{bd}, \tag{6}$$

where P is the load at the initiation of a crack, is the crack length, b is the breadth of the specimen, d is the thickness of the specimen, and Q is the geometry constant.

Q is calculated using the following equation:

$$Q = 1.99 - 0.41\left(\frac{a}{b}\right) + 18.7\left(\frac{a}{b}\right)^2 - 38.48\left(\frac{a}{b}\right)^3 + 53.85\left(\frac{a}{b}\right)^4. \tag{7}$$

The variation of fracture toughness with filler content is also given in Figure 13. The fracture toughness increases negligibly (by 8%) with the addition of TiO_2 at intermediate concentrations. However, when the TiO_2 content was increased to 6.9 wt% there was a dramatic decrease in K_{IC}, even lower than that of the control neat crosslinked epoxy system due to the agglomeration of TiO_2 particles.

FESEM analysis of the fracture surfaces of the TiO_2-filled crosslinked epoxy network composites can give an insight into the cause and location of failure as well as the dispersion state of the particles within the epoxy matrix. Figure 14 shows FESEM micrographs of the samples after the K_{IC} fracture tests. The FESEM fracture micrographs after the tensile, flexural, and impact tests were similar to those of the K_{IC} fractured samples. It is well known that the presence of rigid fillers may induce several toughening mechanisms in epoxy matrices; this includes crack deflection [54, 55], plastic deformation [56, 57], and crack front pinning [58]. Some of these toughening mechanisms was observed the for epoxy/TiO_2 composites. Figure 14(a) shows the fracture surface of the neat, crosslinked epoxy; it reveals a brittle behavior characterized by large smooth areas, typically flat, and the crack propagated uninterrupted in the direction of the applied load. The nanoparticle reinforced composites and on the other hand, exhibited rougher fracture surfaces, as shown in Figures 14(b)–14(d). Nanoparticle agglomerates of

Table 6: Tensile properties of the epoxy modified nanocomposites.

Sample	Tensile strength MPa	Tensile modulus GPa	Tensile elongation %	Ductility (area under the stress/strain curves)
Neat epoxy	51 ± 2	2.3 ± 0.1	3.99 ± 0.2	121
0.7 wt% TiO_2	55 ± 3	2.5 ± 0.1	4.23 ± 0.3	136
3.6 wt% TiO_2	56 ± 3	2.6 ± 0.1	3.88 ± 0.3	124
6.9 wt% TiO_2	57 ± 2	2.7 ± 0.1	4.12 ± 0.2	135

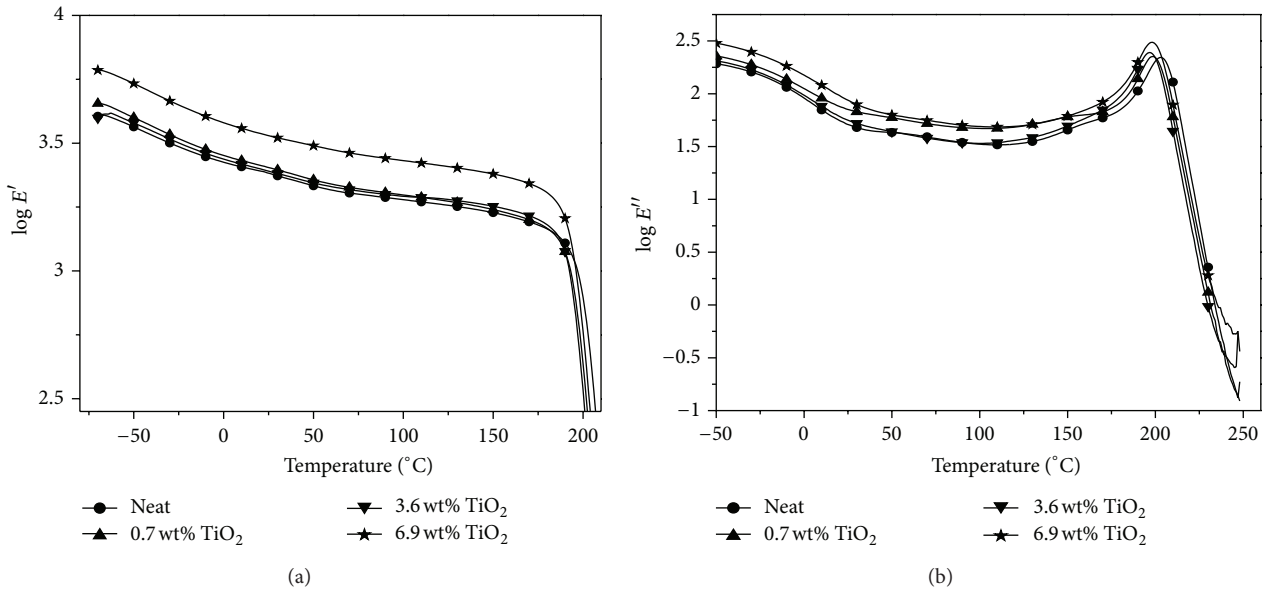

Figure 12: (a) Storage modulus curves for epoxy nanocomposites. (b) Loss modulus curves for epoxy nanocomposites.

Table 7: Flexural properties of the epoxy modified nanocomposites.

Sample	Flexural strength MPa	Flexural modulus MPa	Flexural elongation %
Neat epoxy	110 ± 5.5	3.3 ± 0.2	5.45 ± 0.3
0.7 wt% TiO_2	91 ± 4	3.1 ± 0.1	3.74 ± 0.2
3.6 wt% TiO_2	64 ± 3.7	3.5 ± 0.1	2.03 ± 0.1
6.9 wt% TiO_2	77 ± 3.8	4.2 ± 0.2	2.14 ± 0.1

a few micrometers size can be seen for all the samples along with individual nanoparticles. The FESEM micrographs of the 0.7 wt% filler content reveal the prevention of crack propagation by the agglomerates of TiO_2 and the crack seems to be deviated from the original path and hence more energy is needed for the crack propagation. Some of the TiO_2 particles were pulled out from the epoxy matrix by the application of the external load, so that smooth black holes remain visible (Figure 14(b)). The latter indicates a breakdown of the filler/matrix interface which would reduce interactions between crack and particle and subsequently force the crack to breakaway at lower stresses. This could explain why the measured fracture toughness improvement was low [59].

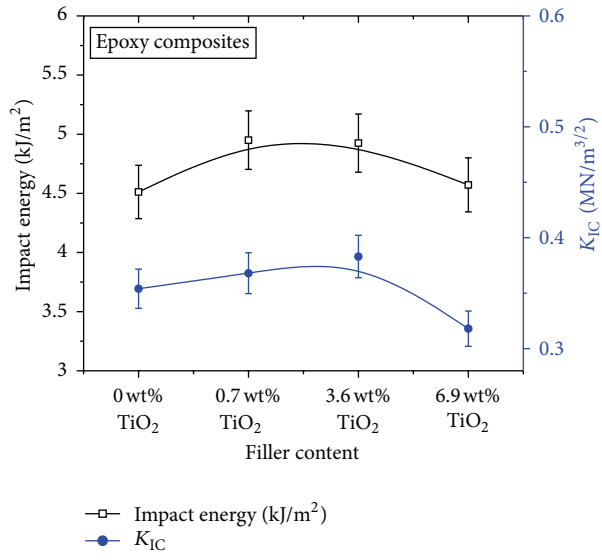

Figure 13: Impact strength and fracture toughness of epoxy nanocomposites.

With increase in particle loading, the number of particles increased; this causes particle-particle interaction rather than the particle-matrix interaction. Hence the particles begin to agglomerate and form lumps which eventually affected the

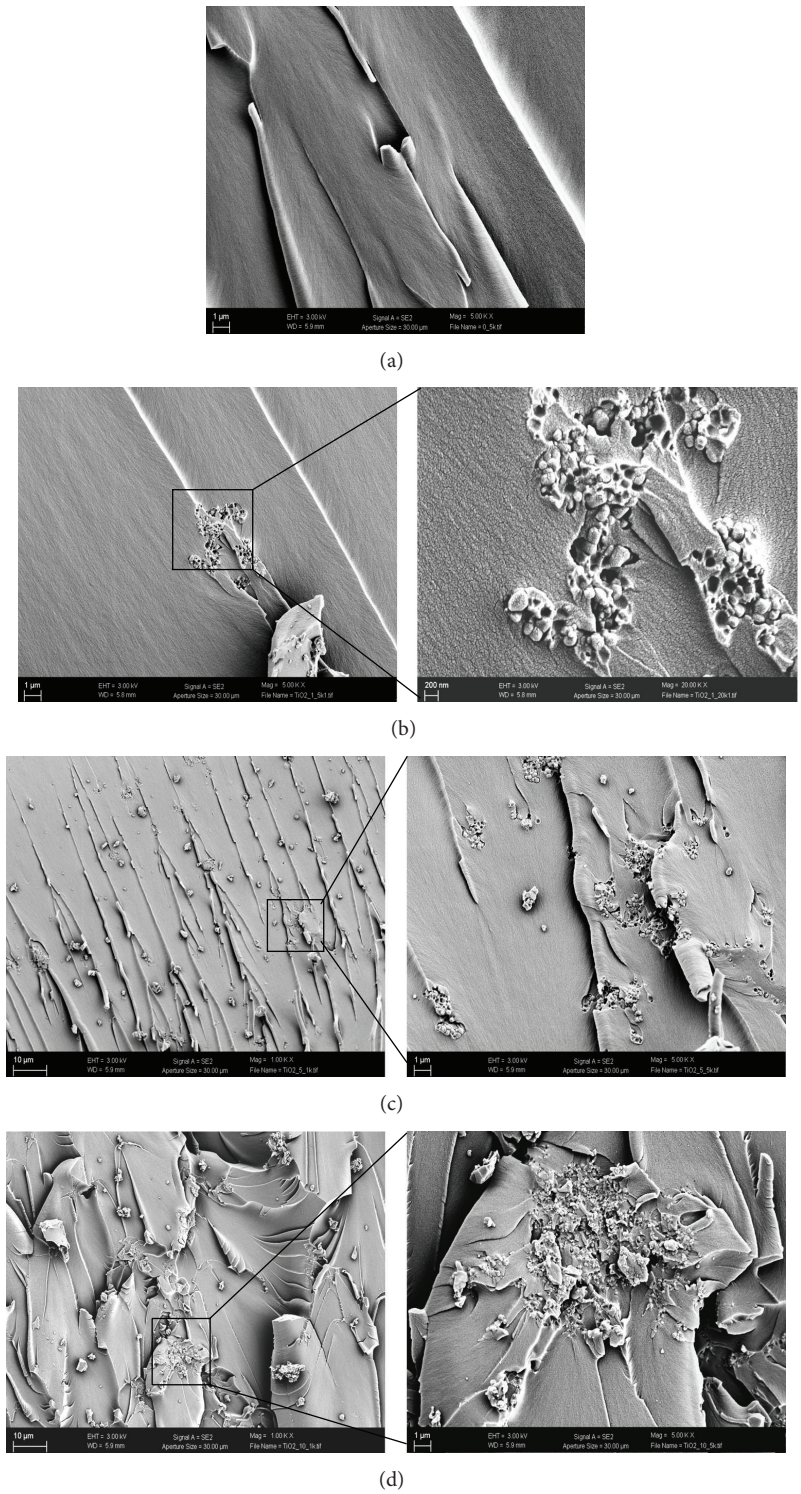

(a)

(b)

(c)

(d)

Figure 14: Scanning electron micrographs of failed surfaces of nanocomposites; (a) neat epoxy, (b) 0.7 wt% TiO_2, (c) 3.6 wt% TiO_2, and (d) 6.9 wt% TiO_2.

van der Waals interaction between the polymer chains and that may cause a decrease in properties. The agglomerates of TiO_2 are believed to cause high stress concentrations in the polymer matrix near the particle edges, which will facilitate failure during the fracture tests. In the case of 3.6 wt% TiO_2 (Figure 14(c)) a morphology similar to 0.7 wt% TiO_2 was observed; the particles are more agglomerated but these agglomerates not act as failure sites and hence better properties compared to neat epoxy. The particle agglomerates remaining in the matrix should be small enough

to not induce a brittle and detrimental failure in the way like "large" particles would. On the other hand, when the concentration was increased to 6.9 wt% TiO_2 (Figure 14(d)), the fracture morphology was quite different from the rest of the samples, with larger particle agglomerates. However, the particle agglomerates were large enough to induce a brittle and detrimental failure in the way "large" particles would do and hence a decline in mechanical properties.

5. Conclusion

The catalytic effect of TiO_2 nanoparticle on epoxy/amine reaction was carefully analyzed using FTIR and DSC studies. This was further confirmed by rheological studies. The gelation time was decreased, with the addition of TiO_2 nanofiller due to the acceleration effect caused by the nanoparticles on the epoxy/amine reaction. PVT studies reveal that small amount of TiO_2 can potentially reduce the volume shrinkage behavior of epoxy. The effect of filler loading on the thermal and mechanical properties and the morphology were investigated. TiO_2 is an effective reinforcement for epoxy system for high performance applications. The thermal expansion behaviour was not influenced by the addition of TiO_2. Similarly, thermal stability was enhanced negligibly by the addition of TiO_2 nanoparticles. The DDS-cured epoxy nanocomposites have a single T_g corresponding to that of the epoxy phase, which shows only minor decrease with TiO_2 content and was close to T_g of the pure cross-linked epoxy system. Storage modulus results reveal better stiffness (40% increase (MPa)) for the 6.9 wt% TiO_2 composites. The rigid TiO_2 particles have no effect or little effect on the mechanical properties of the epoxy system; however, modulus increases at some point. Morphological investigation of the K_{IC} fracture surface indicates that the slight improvement in properties of the composites can be ascribed to the presence of the TiO_2 nanoparticles in the epoxy, which leads to increased surface roughness and hence energy dissipated during the propagation of the crack. However, when the concentration of filler is more than a critical value the particles were more agglomerated and the particle agglomerates are large enough to induce a brittle and detrimental failure.

Conflict of Interests

The authors do not have any direct financial relation with the commercial identities.

Acknowledgments

Jyotishkumar Parameswaranpillai acknowledges the Department of Science and Technology, Government of India, for the financial support under INSPIRE Faculty Fellowship (IFA-CH-16).

References

[1] K. Varma and V. B. Gupta, "Thermosetting resin—properties," *Comprehensive Composite Materials*, vol. 2, pp. 1–56, 2003.

[2] P. Jyotishkumar, J. Pionteck, R. Häßler, S. M. George, U. Cvelbar, and S. Thomas, "Studies on stress relaxation and thermomechanical properties of poly(acrylonitrile-butadiene-styrene) modified epoxy-amine systems," *Industrial & Engineering Chemistry Research*, vol. 50, pp. 4432–4440, 2011.

[3] J. S. Tsuji, A. D. Maynard, P. C. Howard et al., "Research strategies for safety evaluation of nanomaterials, part IV: risk assessment of nanoparticles," *Toxicological Sciences*, vol. 89, no. 1, pp. 42–50, 2006.

[4] M. Antonietti and C. Goltner, "Superstructures of functional colloids: chemistry on the nanometer scale," *Angewandte Chemie*, vol. 36, no. 9, pp. 910–928, 1997.

[5] G. Schmid, "Large clusters and colloids. Metals in the embryonic state," *Chemical Reviews*, vol. 92, no. 8, pp. 1709–1727, 1992.

[6] P. Carballeira and F. Haupert, "Toughening effects of titanium dioxide nanoparticles on TiO_2/epoxy resin nanocomposites," *Polymer Composites*, vol. 31, no. 7, pp. 1241–1246, 2010.

[7] B. Wetzel, F. Haupert, and F. Zhang, "Epoxy nanocomposites with high mechanical and tribological performance," *Composites Science and Technology*, vol. 63, no. 14, pp. 2055–2067, 2003.

[8] R. P. Singh, M. Zhang, and D. Chan, "Toughening of a brittle thermosetting polymer: effects of reinforcement particle size and volume fraction," *Journal of Materials Science*, vol. 37, no. 4, pp. 781–788, 2002.

[9] L. Guadagno, L. Vertuccio, A. Sorrentino et al., "Mechanical and barrier properties of epoxy resin filled with multi-walled carbon nanotubes," *Carbon*, vol. 47, no. 10, pp. 2419–2430, 2009.

[10] G. C. Huang and J. K. Lee, "Isothermal cure characterization of fumed silica/epoxy nanocomposites: the glass transition temperature and conversion," *Composites A*, vol. 41, no. 4, pp. 473–479, 2010.

[11] W. K. Goertzen, X. Sheng, M. Akinc, and M. R. Kessler, "Rheology and curing kinetics of fumed silica/cyanate ester nanocomposites," *Polymer Engineering and Science*, vol. 48, no. 5, pp. 875–883, 2008.

[12] M. Harsch, J. Karger-Kocsis, and M. Holst, "Influence of fillers and additives on the cure kinetics of an epoxy/anhydride resin," *European Polymer Journal*, vol. 43, no. 4, pp. 1168–1178, 2007.

[13] P. Jyotishkumar, J. Pionteck, L. Häußler, G. Adam, and S. Thomas, "A novel hydroxyapatite/ethylene-vinyl acetate/copolymer 66 composite for hard tissue regeneration," *Journal of Macromolecular Science B*, vol. 51, no. 1, pp. 1–11, 2012.

[14] P. Jyotishkumar, S. M. George, P. Moldenaers, and S. Thomas, "Dynamics of phase separation in poly(acrylonitrile-butadiene-styrene)-modified epoxy/DDS system: kinetics and viscoelastic effects," *Journal of Physical Chemistry B*, vol. 114, no. 42, pp. 13271–13281, 2010.

[15] Y. Liu, X. Zhong, and Y. Yu, "Gelation behavior of thermoplastic-modified epoxy systems during polymerization-induced phase separation," *Colloid and Polymer Science*, vol. 288, no. 16-17, pp. 1561–1570, 2010.

[16] M. Holst, K. Schänzlin, M. Wenzel, J. Xu, D. Lellinger, and I. Alig, "Time-resolved method for the measurement of volume changes during polymerization," *Journal of Polymer Science B*, vol. 43, no. 17, pp. 2314–2325, 2005.

[17] J. Jose, K. Joseph, J. Pionteck, and S. Thomas, "PVT behavior of thermoplastic poly(styrene-co-acrylonitrile)-modified epoxy systems: relating polymerization-induced viscoelastic phase separation with the cure shrinkage performance," *Journal of Physical Chemistry B*, vol. 112, no. 47, pp. 14793–14803, 2008.

[18] M. Z. Rong, M. Q. Zhang, H. Liu, H. M. Zeng, B. Wetzel, and K. Friedrich, "Microstructure and tribological behavior of polymeric nanocomposites," *Industrial Lubrication and Tribology*, vol. 53, no. 2, pp. 72–77, 2001.

[19] M. A. L. Manchado, L. Valentini, J. Biagiotti, and J. M. Kenny, "Thermal and mechanical properties of single-walled carbon nanotubes-polypropylene composites prepared by melt processing," *Carbon*, vol. 43, no. 7, pp. 1499–1505, 2005.

[20] M. Avella, M. E. Errico, S. Martelli, and E. Martuscelli, "Preparation methodologies of polymer matrix nanocomposites," *Applied Organometallic Chemistry*, vol. 15, no. 5, pp. 435–439, 2001.

[21] H. R. Dennis, D. L. Hunter, D. Chang, S. Kim, J. L. White, and J. W. Cho, "Nanocomposites: the importance of processing," *Plastics Engineering*, vol. 57, no. 1, pp. 56–60, 2001.

[22] J. W. Cho and D. R. Paul, "Nylon 6 nanocomposites by melt compounding," *Polymer*, vol. 42, no. 3, pp. 1083–1094, 2001.

[23] Q. Wang, H. Xia, and C. Zhang, "Preparation of polymer/inorganic nanoparticles composites through ultrasonic irradiation," *Journal of Applied Polymer Science*, vol. 80, no. 9, pp. 1478–1488, 2001.

[24] T. Adebahr, C. Roscher, and J. Adam, "Reinforcing nanoparticles in reactive resins," *European Coatings Journal*, no. 4, pp. 144–149, 2001.

[25] S. Kang, S. I. Hong, C. R. Choe, M. Park, S. Rim, and J. Kim, "Preparation and characterization of epoxy composites filled with functionalized nanosilica particles obtained via sol-gel process," *Polymer*, vol. 42, no. 3, pp. 879–887, 2001.

[26] G. Xian, R. Walter, and F. Haupert, "A synergistic effect of nano-TiO_2 and graphite on the tribological performance of epoxy matrix composites," *Journal of Applied Polymer Science*, vol. 102, no. 3, pp. 2391–2400, 2006.

[27] M. Sangermano, G. Matucelli, E. Amerio et al., "Preparation and characterization of nanostructured TiO_2/epoxy polymeric films," *Macromolecular Materials and Engineering*, vol. 291, no. 5, pp. 517–523, 2006.

[28] R. J. Nussbaumer, W. R. Caseri, P. Smith, and T. Tervoort, "Polymer-TiO_2 nanocomposites: a route towards visually transparent broadband UV filters and high refractive index materials," *Macromolecular Materials and Engineering*, vol. 288, no. 1, pp. 44–49, 2003.

[29] M. Xiong, S. Zhou, B. O. You, G. U. Guangxin, and L. Wu, "Effect of preparation of titania sol on the structure and properties of acrylic resin/titania hybrid materials," *Journal of Polymer Science B*, vol. 42, no. 20, pp. 3682–3694, 2004.

[30] Y. Tong, Y. Li, F. Xie, and M. Ding, "Preparation and characteristics of polyimide-TiO_2 nanocomposite film," *Polymer International*, vol. 49, no. 11, pp. 1543–1547, 2000.

[31] H. Segawa, K. Tateishi, Y. Arai, K. Yoshida, and H. Kaji, "Patterning of hybrid titania film using photopolymerization," *Thin Solid Films*, vol. 466, no. 1-2, pp. 48–53, 2004.

[32] M. D. Soucek, A. H. Johnson, L. E. Meemken, and J. M. Wegner, "Preparation of nano-sized UV-absorbing titanium-oxo-clusters via a photo-curing ceramer process," *Polymers for Advanced Technologies*, vol. 16, no. 2-3, pp. 257–261, 2005.

[33] P. V. Kamat, "Photochemistry on nonreactive and reactive (semiconductor) surfaces," *Chemical Reviews*, vol. 93, no. 1, pp. 267–300, 1993.

[34] J. C. Yu, W. Ho, J. Yu, H. Yip, and P. K. Wong, "Efficient visible-light-induced photocatalytic disinfection on sulfur-doped nanocrystalline titania," *Environmental Science & Technology*, vol. 39, no. 4, pp. 1175–1179, 2005.

[35] J. C. Yu, W. Ho, J. Lin, H. Yip, and P. K. Wong, "Photocatalytic activity, antibacterial effect, and photoinduced hydrophilicity of TiO_2 films coated on a stainless steel substrate," *Environmental Science & Technology*, vol. 37, no. 10, pp. 2296–2301, 2003.

[36] A. Chatterjee and M. S. Islam, "Fabrication and characterization of TiO_2-epoxy nanocomposite," *Materials Science and Engineering A*, vol. 487, no. 1-2, pp. 574–585, 2008.

[37] K. S. Huang, Y. H. Nien, J. S. Chen, T. R. Shieh, and J. W. Chen, "Synthesis and properties of epoxy/TiO_2 composite materials," *Polymer Composites*, vol. 27, no. 2, pp. 195–200, 2006.

[38] A. A. Wazzan, H. A. Al-Turaif, and A. F. Abdwlkader, "Influence of submicron TiO_2 particles on the mechanical properties and fracture characteristics of cured epoxy resin," *Polymer-Plastics Technology and Engineering* , vol. 45, no. 10, pp. 1155–1161, 2006.

[39] A. Sabra, T. M. Lam, J. P. Pascault, M. F. Grenier-Loustalot, and P. Grenier, "Characterization and behaviour of epoxy-based diaminodiphenylsulphone networks," *Polymer*, vol. 28, no. 6, pp. 1030–1036, 1987.

[40] T. M. Don and J. P. Bell, "Fourier transform infrared analysis of polycarbonate/epoxy mixtures cured with an aromatic amine," *Journal of Applied Polymer Science*, vol. 69, no. 12, pp. 2395–2407, 1998.

[41] P. Jyotishkumar, E. Abraham, S. M. George et al., "Preparation and properties of MWCNTs/poly(acrylonitrile-styrene-butadiene)/epoxy hybrid composites," *Journal of Applied Polymer Science*, vol. 127, no. 4, pp. 3093–3103, 2013.

[42] P. Jyotishkumar, P. Moldenaers, S. M. George, and S. Thomas, "Viscoelastic effects in thermoplastic poly(styrene-acrylonitrile)-modified epoxy-DDM system during reaction induced phase separation," *Soft Matter*, vol. 8, no. 28, pp. 3452–7462, 2012.

[43] W. Gan, G. Zhan, M. Wang, Y. Yu, Y. Xu, and S. Li, "Rheological behaviors and structural transitions in a polyethersulfone-modified epoxy system during phase separation," *Colloid and Polymer Science*, vol. 285, no. 15, pp. 1727–1731, 2007.

[44] S. Poncet, G. Boiteux, J. P. Pascault et al., "Monitoring phase separation and reaction advancement in situ in thermoplastic/epoxy blends," *Polymer*, vol. 40, no. 24, pp. 6811–6820, 1999.

[45] S. Swier and B. van Mele, 1998, Polymer Network Preprints P12, Trondheim.

[46] I. Alig and W. Jenninger, "Curing kinetics of phase separating epoxy thermosets studied by dielectric and calorimetric investigations: a simple model for the complex dielectric permittivity," *Journal of Polymer Science B*, vol. 36, no. 13, pp. 2461–2470, 1998.

[47] J. K. Gillham and P. G. Babayevsky, "Epoxy thermosetting systems: dynamic mechanical analysis of the reactions of aromatic diamines with the diglycidyl ether of bisphenol A," *Journal of Applied Polymer Science*, vol. 17, no. 7, pp. 2067–2088, 1973.

[48] P. A. Oyanguren and R. J. J. Williams, "Cure of epoxy novolacs with aromatic diamines. I. Vitrification, gelation, and reaction kinetics," *Journal of Applied Polymer Science*, vol. 47, no. 8, pp. 1361–1371, 1993.

[49] J. M. Barton, D. C. L. Greenfield, and K. A. Hodd, "Some effects of structure on the cure of glycidylether epoxy resins," *Polymer*, vol. 33, no. 6, pp. 1177–1186, 1992.

[50] P. J. Flory, *Principles of Polymer Chemistry*, Universidad de Cornell, Ithaca, NY, USA, 1953.

[51] P. Jyotishkumar, J. Pionteck, C. Özdilek et al., "Rheology and pressure-volume-temperature behavior of the thermoplastic poly(acrylonitrile-butadiene-styrene)-modified epoxy-DDS system during reaction induced phase separation," *Soft Matter*, vol. 7, no. 16, pp. 7248–7256, 2011.

[52] J. A. Ramos, N. Pagani, C. C. Riccardi, J. Borrajo, S. N. Goyanes, and I. Mondragon, "Cure kinetics and shrinkage model for epoxy-amine systems," *Polymer*, vol. 46, no. 10, pp. 3323–3328, 2005.

[53] P. Jyotishkumar, E. Logakis, S. M. George et al., "Preparation and properties of multiwalled carbon nanotube/epoxy-amine composites," *Journal of Applied Polymer Science*, vol. 127, no. 4, pp. 3063–3073, 2013.

[54] K. T. Faber and A. G. Evans, "Crack deflection processes—I. Theory," *Acta Metallurgica*, vol. 31, no. 4, pp. 565–576, 1983.

[55] K. T. Faber and A. G. Evans, "Crack deflection processes—II. Experiment," *Acta Metallurgica*, vol. 31, no. 4, pp. 577–584, 1983.

[56] T. Kawaguchi and R. A. Pearson, "The moisture effect on the fatigue crack growth of glass particle and fiber reinforced epoxies with strong and weak bonding conditions, part 2: a microscopic study on toughening mechanism," *Composites Science and Technology*, vol. 64, no. 13-14, pp. 1991–2007, 2004.

[57] A. J. Kinloch, D. Maxwell, and R. J. Young, "Micromechanisms of crack propagation in hybrid-particulate composites," *Journal of Materials Science Letters*, vol. 4, no. 10, pp. 1276–1279, 1985.

[58] J. Spanoudakis and R. J. Young, "Crack propagation in a glass particle-filled epoxy resin," *Journal of Materials Science*, vol. 19, no. 2, pp. 473–486, 1984.

[59] B. Wetzel, P. Rosso, F. Haupert, and K. Friedrich, "Epoxy nanocomposites—fracture and toughening mechanisms," *Engineering Fracture Mechanics*, vol. 73, no. 16, pp. 2375–2398, 2006.